Paper

Modeling of Microwave Cavities Based on SIBC-FDTD Method for EM Wave Focalization by TR Technique

Zhigang Li[1], Younes Aimer[2], and Tayeb H. C. Bouazza[3]

[1]*ESECA, Department of ENSEEIHT, National Polytechnic, Institute of Toulouse, Toulouse, France,*
[2]*Mines Saint-Etienne, Centre of Microelectronics in Provence, Department of Flexible Electronics, Gardanne, France,*
[3]*XLIM Laboratory UMR-CNRS 7252, Institute of Technology of Angouleme, University of Poitiers, Poitiers, France*

https://doi.org/10.26636/jtit.2022.153021

Abstract — The time reversal (TR) techniques used in electromagnetics have been limited for a variety of reasons, including extensive computations, complex modeling and simulation, processes as well as, large-scale numerical analysis. In this paper, the SIBC-FDTD method is applied to address these issues and to efficiently model TR systems. An original curvilinear modeling method is also proposed for constructing various obstacles in a 2D microwave cavity and for processing the corners of the cavity. The EM waves' spatio-temporal focalization has been realized, and results of the simulations further prove the accuracy and effectiveness of this modeling method. Furthermore, they demonstrate that the microwave cavity processes may significantly improve the focalization quality in terms of SSLL enhancement.

Keywords — curvilinear modeling, EM waves focalization, SIBC-FDTD method, TR technique.

1. Introduction

The time-reversal technique was first proposed by Bogert from Bell Labs in 1957. In 2005, Lerosey *et al.* introduced the TR's spatio-temporal focalization in electromagnetics [1]. In their experiments, electromagnetic wave signals emitted by the antenna were recorded by a receiving antenna known as the time-reversal mirror (TRM). The recorded signal was time-reversely retransmitted by the TRM, thus resulting in focalization of EM waves at the initial position of the transmitting antenna. In recent years, more researches have focused on the applications of this phenomenon, e.g. in the fields of acoustics [2]–[3], medicine [4]–[5], and communications [6]–[9].

To simulate the propagation of an EM wave throughout the entire TR process, the finite-difference time-domain (FDTD) method, one of the most effective numerical calculation methods, has been widely used [10]–[13]. Its main idea is to transform the propagation of EM waves into spatial and temporal propulsion by discretizing Maxwell equations. It needs to be borne in mind that boundary conditions are also critical for simulating propagation of EM waves in a confined space. However, since good conductors have a low skin depth and sharp field variations, a tiny grid is required to calculate the distribution of the EM field on their surfaces, which significantly increases computational complexity. To solve this problem, researchers have introduced the surface impedance boundary condition (SIBC) to the FDTD method. This method can directly obtain the field distribution at the interface without considering the interior of the conductor, thus drastically improving computation efficiency.

In 1992, Maloney *et al.* proposed an efficient implementation of SIBC in the FDTD method based on exponential approximation, and various experiments have demonstrated its applicability [14]. However, the degree of computational complexity failed to decrease significantly.

In recent years, Mao *et al.* have constructed a new absorbing boundary condition by setting surface impedance to free space in order to terminate the outer boundary of the FDTD computational domain [15]–[16]. This approach dramatically reduced computational complexity without affecting the level of accuracy.

Based on these facts, this study aims to contribute to this increasingly popular area by exploring more effective methods for modeling TR systems.

The paper in organized as follows. Section 2 presents the derived theoretical formulas of the SIBC-FDTD method, which can be used to model the EM wave propagation process, microwave cavities, and obstacles. It continues by explaining the principle of TR modeling and shows how this approach naturally leads to focalization. In Section 3, several simulations are conducted to verify effectiveness of the modelling method and to demonstrate how the presented cavity improves the quality of focalization. Furthermore, a series of parallel simulations is performed to re-validate this conclusion by employing two customized metrics, namely side-lobe level (SLL) and spatial side-lobe level (SSLL).

2. TR System Modeling Approach

2.1. EM Wave Propagation Modeling

With Maxwell's equations serving as a point of departure, time-domain propulsion formulas for the FDTD method may be obtained by performing the central difference and discrete

approximation to its differential form. Thus, the continuous electromagnetic wave propagation problem is converted into a discrete numerical problem, which is well suited to deal with electromagnetic field calculations in large and complex structures.

Assuming that the study space is passive and that electrical and magnetic losses are not considered, the Maxwell time-domain differential equations used for constructing the FDTD algorithm can be expressed as:

$$\nabla \times \vec{H} = \frac{\partial \vec{D}}{\partial t}, \tag{1}$$

$$\nabla \times \vec{E} = -\frac{\partial \vec{B}}{\partial t}, \tag{2}$$

where $\vec{E}$ is the electric field intensity in V/m, $\vec{H}$ is the magnetic field intensity in A/m, $\vec{B}$ is the magnetic flux density in Wb/m^2, and $\vec{D}$ is the electric displacement in C/m^2.

Besides, constitutive relations are essential to complement Maxwell's equations and describe the medium's properties. The constitutive relations for linear, isotropic and non-dispersive media can be written as:

$$\vec{D} = \varepsilon \cdot \vec{E}, \tag{3}$$

$$\vec{B} = \mu \cdot \vec{H}, \tag{4}$$

where ε is the permittivity of the medium in F/m, μ is the permeability in H/m.

In solving the one-dimensional (1D) problem, it is assumed that the electromagnetic wave propagates along the x-axis, so both E_x and H_x are equal to zero, and Maxwell's equations can be simplified as:

$$\frac{\partial E_z}{\partial x} = \mu \frac{\partial H_y}{\partial t}, \tag{5}$$

$$\frac{\partial H_y}{\partial x} = \epsilon \frac{\partial E_z}{\partial t}. \tag{6}$$

It can be noticed that the left and right-hand sides of the equation are space and time partial derivative term, respectively. The distribution of E_z and H_y in the 1D Yee cell is given in Fig. 1. In space and time dimensions, the $\vec{E}$ and $\vec{H}$ components are staggered at an interval of half the grid length, an essential basis for the FDTD method's iteration.

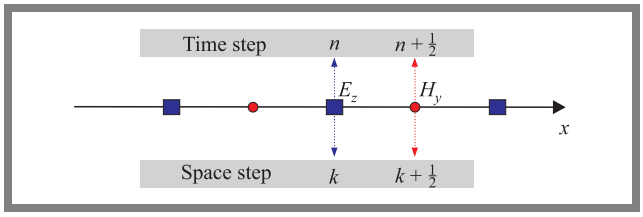

Fig. 1. Distribution of E_z and H_y in the 1D Yee cell.

By using Taylor formulas, the discrete form of Eqs. (5) and (6) can be achieved as:

$$H_y^{n+\frac{1}{2}}\left(k+\frac{1}{2}\right) = H_y^{n-\frac{1}{2}}\left(k+\frac{1}{2}\right) + \frac{\Delta t}{\mu \Delta x}\left[E_z^n(k+1) - E_z^n(k)\right], \tag{7}$$

$$E_z^{n+1}(k) = E_z^n(k) + \frac{\Delta t}{\epsilon \Delta x}\left[H_y^{n+\frac{1}{2}}\left(k+\frac{1}{2}\right) - H_y^{n+\frac{1}{2}}\left(k-\frac{1}{2}\right)\right]. \tag{8}$$

Moreover, because FDTD is an infinite approximation method, stability conditions must be set to ensure the convergence of the solution. The size of the grid must also be limited to reduce errors. The relationship is given by:

$$\delta \leqslant \frac{\lambda_{\min}}{10}, \tag{9}$$

$$c \cdot \Delta t \leqslant \frac{1}{\sqrt{(\frac{1}{\Delta x})^2 + (\frac{1}{\Delta y})^2 + (\frac{1}{\Delta z})^2}}, \tag{10}$$

where $\delta = \min[\Delta x, \Delta y, \Delta z]$ and $\lambda_{\min}$ is the minimum wavelength in the computational frequency range, Δx, Δy and Δz are the space steps, Δt is the time step, and c is the speed of light.

Assuming $\Delta x = \Delta y = \Delta z$, the relationship can be replaced like $c \cdot \Delta t \leqslant \delta$, $c \cdot \Delta t \leqslant \frac{\delta}{\sqrt{2}}$ and $c \cdot \Delta t \leqslant \frac{\delta}{\sqrt{3}}$ for 1D, 2D and 3D, respectively. This means that the time interval must not be greater than the time it takes for the wave to pass through one Yee cell at the speed of light.

2.2. 1D SIBC-FDTD Iterative Formulations for Microwave Cavities Modeling

SIBC describes the relationship between the tangential electric field and the tangential magnetic field at two different media interfaces in the frequency domain. The first-order SIBC in the frequency domain is given by:

$$\vec{E}(\omega) = Z_s(\omega)[\vec{n} \times \vec{H}(\omega)], \tag{11}$$

where $s = j\omega$, ω is the angular frequency, $Z_s(\omega)$ is the surface impedance of the conductor, $\vec{n}$ is a unit vector normal to the surface of the lossy metal. Since the surface impedance of a good conductor is

$$Z_s(\omega) = (1+j)\sqrt{\frac{\omega\mu}{2\sigma}} = \sqrt{\frac{j\omega\mu}{\sigma}}, \tag{12}$$

$Z_s(\omega)$ can be separated into the sum of surface resistance $R_s(\omega)$ and surface inductance $L_s(\omega)$ as:

$$Z_s(\omega) = R_s(\omega) + j\omega L_s(\omega). \tag{13}$$

At a specific frequency, $R_s(\omega)$, $L_s(\omega)$ can be treated as approximate constants, as $R_s(\omega) = \sqrt{\frac{\omega\mu}{2\sigma}}$, $L_s(\omega) = \sqrt{\frac{\mu}{2\sigma\omega}}$. Hence, Eq. (11) can be rewritten as:

$$\vec{E}(\omega) = [R_s + j\omega L_s][\vec{n} \times \vec{H}(\omega)]. \tag{14}$$

By using the inverse Fourier transform, the relationship between $\vec{E}$ and $\vec{H}$ can be expressed in the time domain as:

$$\vec{E}(t) = \left[R_s + L_s\frac{\partial}{\partial t}\right]\left[\vec{n} \times \vec{H}(t)\right]. \tag{15}$$

Hence, the schematic diagram of the SIBC-FDTD method in the 1D case may be shown in Fig. 2.

In the FDTD iteration formulas, by replacing the differential operations of $E_z(1+\frac{1}{2})$ and $E_z(n\Delta x + \frac{1}{2})$ in the space with

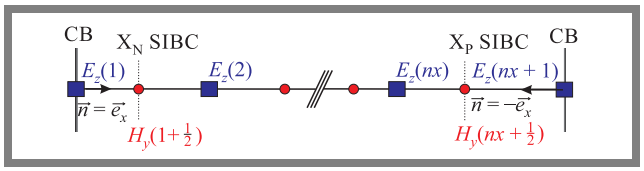

Fig. 2. Schematic diagram of the 1D SIBC-FDTD method.

a half-cell step, the Faraday-Maxwell law can be derived in the following form:

$$H_y^{n+\frac{1}{2}}\left(1+\frac{1}{2}\right)=\frac{\mu\Delta x-\Delta tR_s+2L_s}{\mu\Delta x+\Delta tR_s+2L_s}H_y^{n-\frac{1}{2}}\left(1+\frac{1}{2}\right)+\frac{2\Delta t}{\mu\Delta x+\Delta tR_s+2L_s}E_z^n(2), \tag{16}$$

$$H_y^{n+\frac{1}{2}}\left(n\Delta x+\frac{1}{2}\right)=\frac{\mu\Delta x-\Delta tR_s+2L_s}{\mu\Delta x+\Delta tR_s+2L_s}H_y^{n-\frac{1}{2}}\left(n\Delta x+\frac{1}{2}\right)+\frac{2\Delta t}{\mu\Delta x+\Delta tR_s+2L_s}E_z^n(n\Delta x). \tag{17}$$

2.3. 2D SIBC-FDTD Iterative Formulations for Microwave Cavities Modeling

In the case of 2D (TM wave) scenario, the fundamental components comprise H_x, H_y, and E_z. The schematic diagram of the 2D SIBC-FDTD method is similar to [16], as shown in Fig. 3.

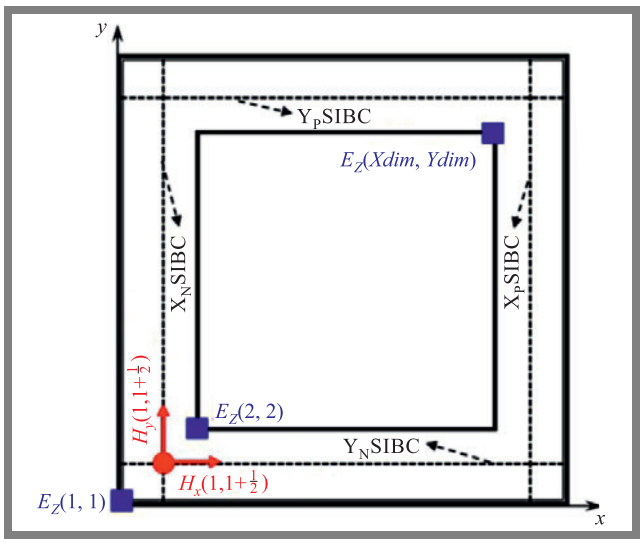

Fig. 3. Schematic diagram of the 2D SIBC-FDTD method.

For any Yee cell on the x-axis negative boundary (X_N SIBC), only H_y existed. The geometry is shown in Fig. 4.

By applying the SIBC equation:

$$E_z\left(1+\frac{1}{2},j\right)=R_sH_y\left(1+\frac{1}{2},j\right)+L_s\frac{\partial H_y\left(1+\frac{1}{2},j\right)}{\partial t}$$

in FDTD, the derived iteration formula on X_N is shown in Eq. (18). Similarly, the iterative recipes on X_P, Y_N and Y_P can be denoted in Eqs. (19), (20), (21), respectively.

$$X=\frac{\mu\Delta x-\Delta tR_s+2L_s}{\mu\Delta x+\Delta tR_s+2L_s}H_y^{n-\frac{1}{2}},$$

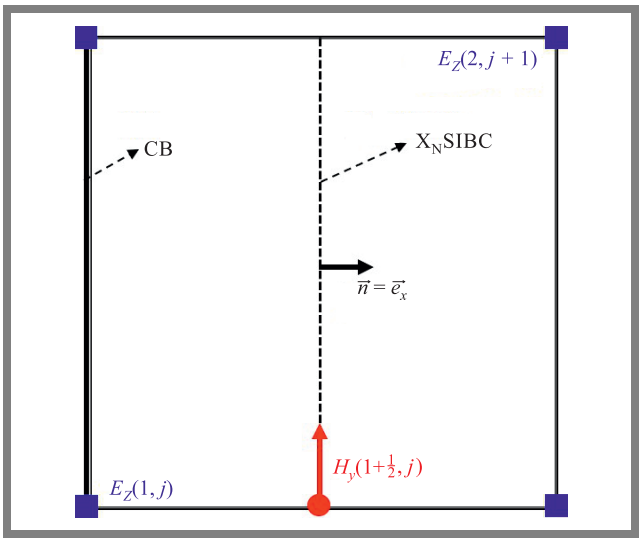

Fig. 4. 2D Yee cell.

$$Y=\frac{\mu\Delta y-\Delta tR_s+2L_s}{\mu\Delta y+\Delta tR_s+2L_s}H_x^{n-\frac{1}{2}},$$

$$H_y^{n+\frac{1}{2}}\left(1+\frac{1}{2},j\right)=X\left(1+\frac{1}{2},j\right)+\frac{2\Delta t}{\mu\Delta x+\Delta tR_s+2L_s}E_z^n(2,j), \tag{18}$$

$$H_y^{n+\frac{1}{2}}\left(x_{\text{dim}}+\frac{1}{2},j\right)=X\left(x_{\text{dim}}+\frac{1}{2},j\right)-\frac{2\Delta t}{\mu\Delta x+\Delta tR_s+2L_s}E_z^n(x_{\text{dim}},j), \tag{19}$$

$$H_x^{n+\frac{1}{2}}\left(i,1+\frac{1}{2}\right)=Y\left(i,1+\frac{1}{2}\right)-\frac{2\Delta t}{\mu\Delta y+\Delta tR_s+2L_s}E_z^n(i,1), \tag{20}$$

$$H_x^{n+\frac{1}{2}}\left(i,y_{\text{dim}}+\frac{1}{2}\right)=Y\left(i,y_{\text{dim}}+\frac{1}{2}\right)+\frac{2\Delta t}{\mu\Delta y+\Delta tR_s+2L_s}E_z^n(i,y_{\text{dim}}). \tag{21}$$

2.4. Curvilinear Modeling

Unlike linear modeling of the microwave cavity, curvilinear modeling is more complicated due to the lack of apparent boundaries in processing corners and constructing obstacles. The solution is to create a matrix of the same dimension corresponding to E_z (blue dots) and to assign E_z values to the matrix as the basis for determining boundaries, as shown in Fig. 5:

$$E_z[i,j]=\begin{cases}0 & \text{if } E_z \text{ is inside the obstacle}\\ 1 & \text{if } E_z \text{ is outside the obstacle}\end{cases}. \tag{22}$$

For example, if the blue dot is inside the obstacles, the matrix's corresponding point will be allocated a 1. Otherwise, it will be a 0.

Determination of the boundary location requires judging the values of two adjacent points in the matrix as shown in

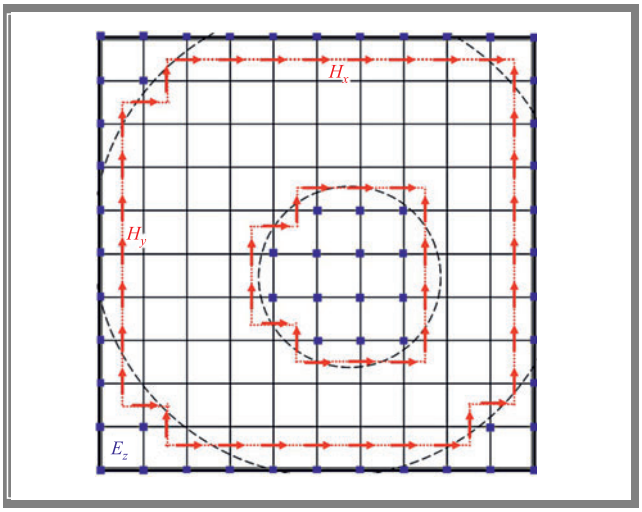

Fig. 5. Schematic diagram of the curvilinear modeling method.

Eq. (23). If the values of two adjacent points on the same row are different, the H_y iteration formula should be utilized as the boundary condition. Similarly, if the values of two adjacent points on the same column are different, the H_x iteration formula should be adopted:

$$\begin{cases} H_x\left[i, j+\frac{1}{2}\right] \text{ is the boundary, if } E_z[i,j] \neq E_z[1,j+1] \\ H_y\left[i+\frac{1}{2}, j\right] \text{ is the boundary, if } E_z[i,j] \neq E_z[i+1,j] \end{cases}. \quad (23)$$

It follows from Fig. 5 that the area enclosed by the red arrow (H_x, H_y) inside the cavity is the modeling circular obstacle, and the area surrounded by the red arrow on the cavity's boundary is the cavity after the corner has been processed.

2.5. Time Reversal Modeling

The complete TR experiment is usually divided into two stages [17]–[18], the forward stage and the backward stage,

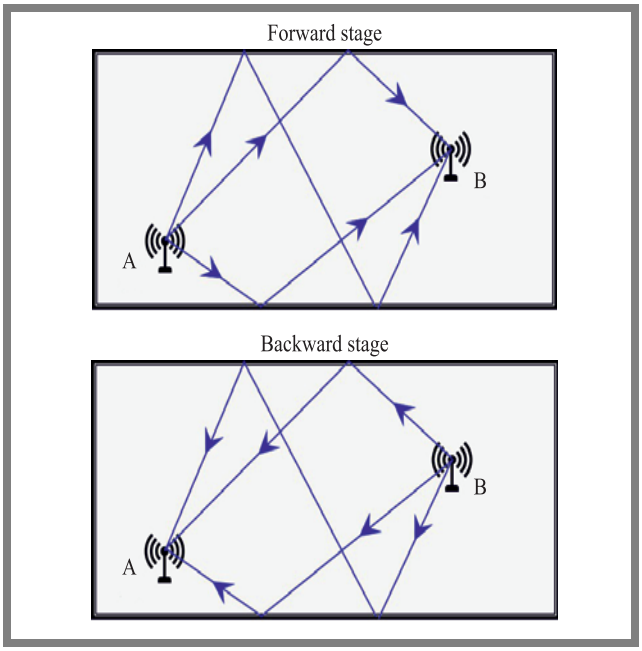

Fig. 6. TR system.

as shown in Fig. 6. During the forward stage, the EM waves signal emitted by source A is received and recorded by the antenna placed at B (TRM) after complex propagation and reflection in the cavity. During the backward stage, the first action is to reverse the signal received at B on the time axis and then the reversed signal is retransmitted, meaning that the signal received at B first will be emitted last.

Then the reversed signal will be focused at source A after a while (approximately the length of the receiving time). This process is known as spatio-temporal focalization characteristic of the TR technique.

3. Simulation Results and Discussion

3.1. Simulation Settings

In this TR simulation, the volume of the metallic microwave cavity is 1.165×1.165 m^2, and the total cavity space is divided into 104×104 grids according to the FDTD stability conditions. Hence, the pixel size used for SIBC-FDTD iteration is approximately 0.0113 m. Moreover, a Gaussian pulse signal is excited at the initial source point A, as shown in Fig. 7. The pulse duration is 8 ns, the carrier frequency is 2.4 GHz, and the amplitude pulse is 10^4 V/m.

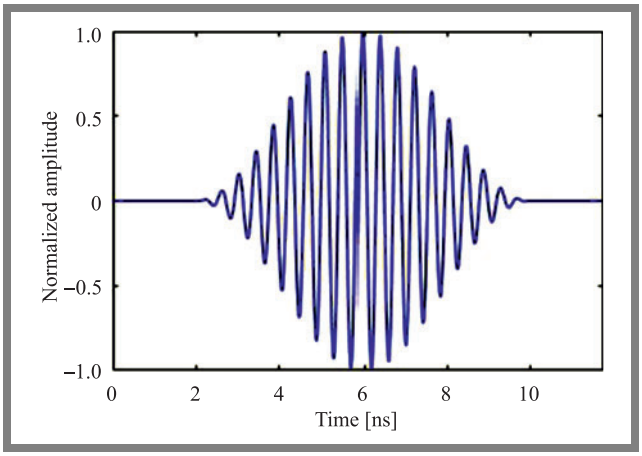

Fig. 7. Initial Gaussian pulse.

Moreover, the signal received by the TRM at point B during the forward stage is shown in Fig. 8. Due to the loss of the cavity's metallic boundaries, the TRM receives a series of signals whose amplitude decays gradually.

To evaluate the focalization quality in the time domain and frequency domain, we have defined such parameters as side-lobe level (SLL) and spatial side-lobe level (SSLL), respectively. SLL refers to the ratio between the first maximum amplitude and the second maximum amplitude of the signal recorded at focalization point A. SSLL, in turn, refers to the ratio between the first spatial maximum amplitude and the second spatial maximum amplitude inside the cavity.

Furthermore, to verify the effectiveness of the curvilinear modeling method and to assess the relationship between cavity complexity and focalization quality, we have set up two in-

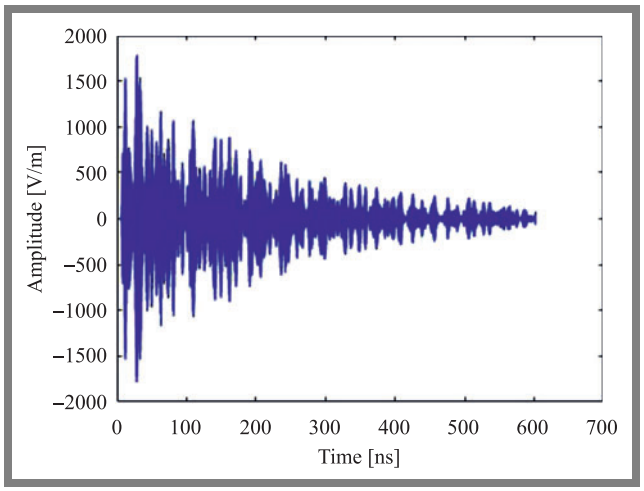

Fig. 8. Recorded signals by TRM at point B.

dependent groups: group 1 with no processing corners and no obstacles, and group 2 with processing corners and obstacles.

3.2. Analysis of Simulation Results

Inside the modeled microwave cavity, the processed corners and the circular obstacle generated using the SIBC-FDTD method can be observed directly in Fig. 9b. Simultaneously, there is no EM wave propagation outside the SIBC boundary, which is in agreement with our modeling theory. Also, at 604.03 ns, the temporal EM wave focalization is more clearly visualized in the group 2 (Fig. 9b) than in group 1 (Fig. 9a).

Figures 10 and 11 quantitatively show the entire focalization process from 0 ns to 604.03 ns. With the reflection of the EM wave emitted from TRM (point B) inside the cavity, the energy gradually accumulates at point A and finally focuses here. Furthermore, by comparing the two figures on the (a) side (group 1), one may notice that additional focalization points exist inside the cavity, for example, at the time points of 350 ns, 480 ns, 530 ns, 560 ns and 590 ns, which means that energy distribution is more dispersed. The comparison of the two figures on the (b) side (group 2) demonstrates that no other apparent focalization points are created and most of the energy is refocused at point A.

Table 1 shows the values of SLL and SSLL obtained from Figs. 10 and 11. Both are boosted more in group 2 than in group 1, which means that the focalization quality is optimized. This is caused by the fact that the first maximum amplitude in group 2 significantly increases to 2434 V/m due to the complex cavity environment reducing the propagation losses.

Tab. 1. Group 1 vs. group 2.

Parameters		Group 1	Group 2
Fig. 10	E_z first peak	713.4 V/m	2434 V/m
	E_z second peak	289.7 V/m	919.2 V/m
	SLL	2.46	2.64
Fig. 11	E_z first peak	988.8 V/m	2434 V/m
	E_z second peak	932.1 V/m	1260 V/m
	SSLL	1.06	1.93

Another possible explanation is that the processed corners and the obstacle have increased propagation complexity, relatively decreasing the EM waves' resonance losses in the rectangular cavity. Group 2 also offers better spatial focalization quality with an SSLL value of approx. 1.93. Most of the emitted energy is refocused at the position of the initial source, except for the boundary loss.

To further validate the modeling approach and the results obtained, two other parallel simulations of group 3 and group 4 are performed by randomly changing the position of the inserted obstacles. The results are shown in Table 2.

It should be highlighted that, compared with group 1, the first maximum amplitude of both group 3 and group 4 increases significantly, which fits in with our earlier observations, proving that the amplitude of the focalization point is positively correlated with cavity complexity. Also, the SLL values are equal to 2 or higher for all groups, meaning that the TR technique's temporal focalization quality is not easily influenced by the external environment, which is an inherent advantage of the TR technique itself. One may also notice that SSLL values are greatly improved for both group 3 and group 4, resulting in better spatial focalization quality.

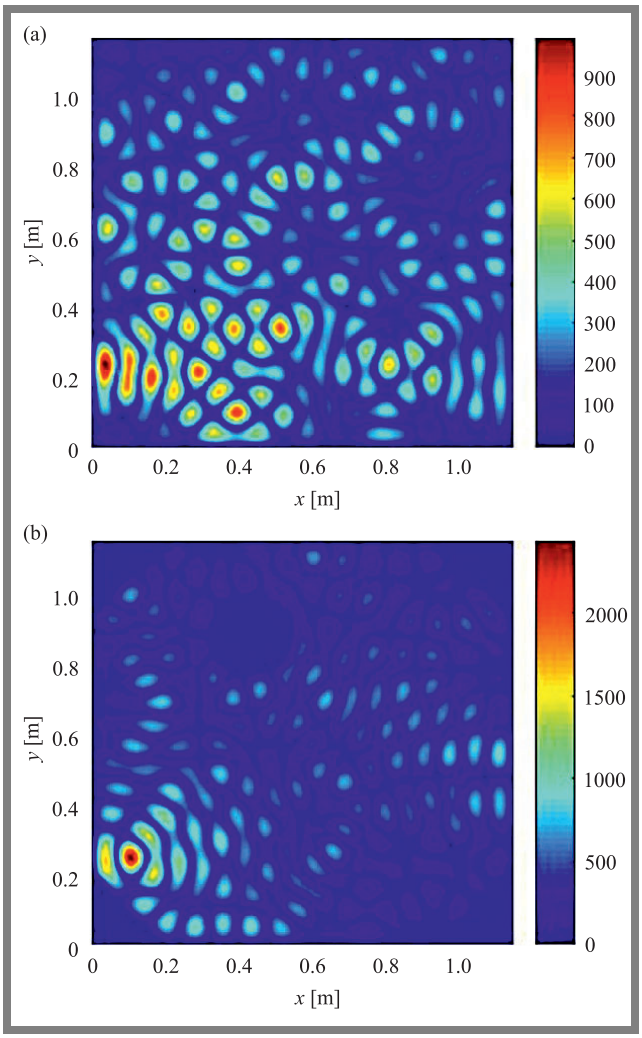

Fig. 9. Focalization point A for E_z at 604.03 ns: a) group 1 and b) group 2.

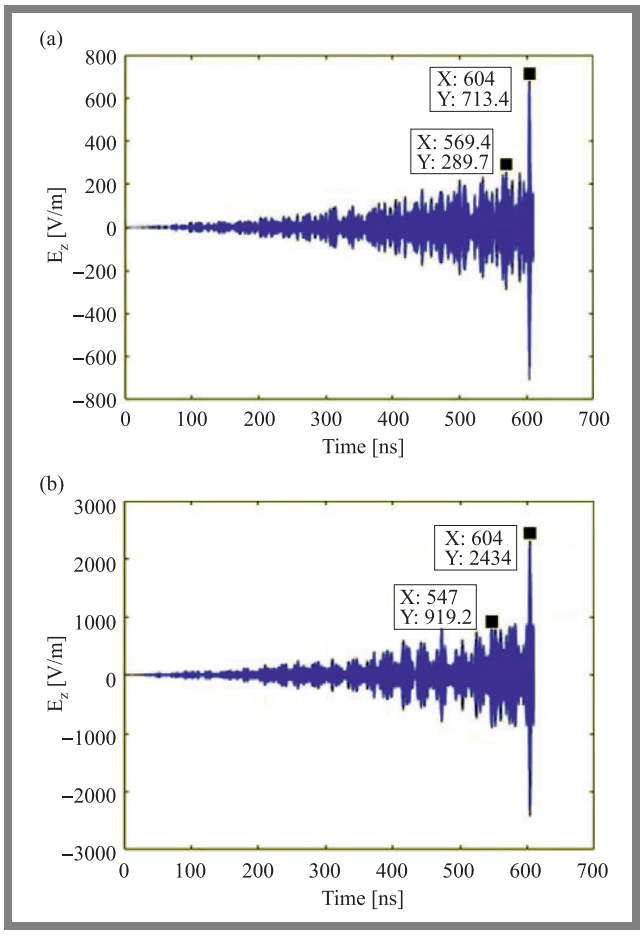

Fig. 10. Signal recorded at focalization point A: a) group 1 and b) group 2.

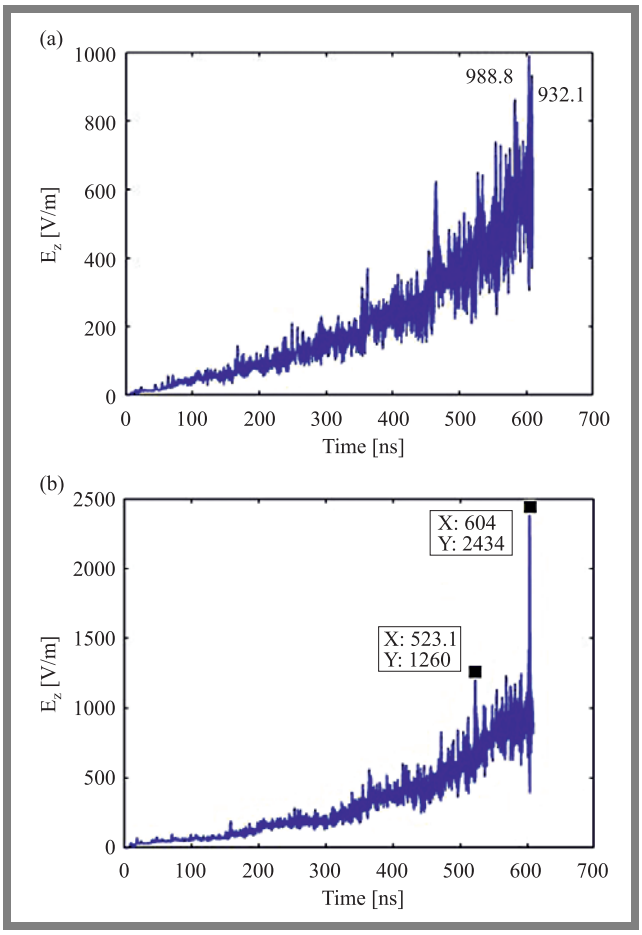

Fig. 11. Maximum amplitude recorded inside the cavity: a) group 1 and b) group 2.

Three additional sets of simulations were completed by randomly changing the TRM position ten times in order to assess the effect of the modeled cavity on the focalization quality. For each set of simulations, the position of the initial source A remains fixed. In addition, the inserted obstacle and the processed corner positions are the same for all simulation groups, and the cavity is left untreated for all reference groups. SLL and SSLL results are shown in Fig. 12.

The yellow/blue dots and the purple/green dots represent the SLL and SSLL values for each independent simulation, respectively. The yellow/purple dots and blue/green dots correspond to the results of the reference and simulation groups. The black and red lines refer to the average values of SLL and

Tab. 2. Results of repeated simulations with randomly changed obstacle location.

Parameters	Group 1	Group 3	Group 4
E_z first peak	713.4 V/m	1990 V/m	1946 V/m
E_z second peak	289.7 V/m	935.6 V/m	993.8 V/m
SLL	2.46	2.13	1.96
E_z first peak	988.8 V/m	1990 V/m	1990 V/m
E_z second peak	932.1 V/m	1322 V/m	1104 V/m
SSLL	1.06	1.51	1.80

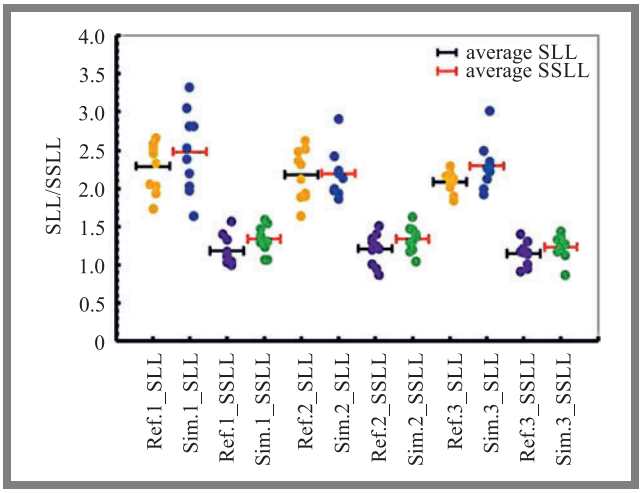

Fig. 12. Average SLL and SSLL of the reference and simulation groups by randomly changing the location of TRM B.

SSLL. What is striking about this chart is that the simulation group reported significantly more SLL and SSLL average values than the reference group, which further verifies the positive correlation between the cavity's complexity and the focalization quality. However, for a single simulation, the difference observed in this study was not significant. This discrepancy could be attributed to the cavity's ergodicity, mean-

ing that our cavity is not complex enough. The round obstacle and arc-shaped corners cannot fully guarantee an improved focalization quality at all locations throughout the cavity.

4. Conclusion

This study was undertaken to model microwave cavities and obstacles and to realize the EM waves' spatio-temporal focalization in 2D. The most prominent finding that has emerged from the research concerned is that the derived SIBC-FDTD method's effectiveness and the original curvilinear modeling method. Obviously, when compared with other methods, such as conventional FDTD, PML-FDTD, etc., this approach will greatly reduce the computation complexity and CPU time due to the reasonable neglect of the outer solution space of the boundaries. Meanwhile, it has been one of the first attempts to thoroughly examine the SIBC-FDTD method in TR simulations. Multiple simulation results obtained in the course of this study also indicate that the processed corners and the inserted obstacle can significantly complicate the propagation environment, which will further improve focalization quality.

Despite these promising results, there is abundant room for further progress in determining the effect of different sizes, shapes of obstacles and even cavities on focalization quality. Meanwhile, further research should be undertaken to investigate the TR system's modeling using the SIBC-FDTD method in 3D.

References

[1] G. Lerosey *et al.*, "Time reversal of electromagnetic waves and telecommunication", *Radio Science*, vol. 40, pp. 1–10, 2005 (DOI: 10.1029/2004RS003193).

[2] Q. Li, C. He, Q. Zhang, and K. Cheng, "Passive time reversal based hybrid time-frequency domain equalizer for underwater acoustic communication", *2016 IEEE International Conference on Signal Processing, Communications and Computing (ICSPCC)*, pp. 1–6, 2016 (DOI: 10.1109/ICSPCC.2016.7753713).

[3] H. Karami, F. Rachidi, M. Azadifar, and M. Rubinstein, "An Acoustic Time Reversal Technique to Locate a Partial Discharge Source: Two-Dimensional Numerical Validation", *IEEE Transactions on Dielectrics and Electrical Insulation*, vol. 27, pp. 2203–2205, 2020 (DOI: 10.1109/TDEI.2020.008837).

[4] M. D. Hossain and A. S. Mohan, "A comparative study of coherent time reversal minimum variance beamformers for breast cancer detection", *2015 9th European Conference on Antennas and Propagation (EuCAP)*, pp. 1–5, 2015 (https://opus.lib.uts.edu.au/bitstream/10453/138599/4/Binder1.pdf).

[5] Y. Tao, T. Mu, and Y. Song, "Time reversal microwave imaging method based on SF-ESPRIT for breast cancer detection", *2017 3rd IEEE International Conference on Computer and Communications (ICCC)*, pp. 2094–2098, 2017 (DOI: 10.1109/CompComm.2017.8322906).

[6] R. C. Qiu, C. Zhou, N. Guo, and J. Q. Zhang, "Time Reversal With MISO for Ultrawideband Communications: Experimental Results", *IEEE Antennas and Wireless Propagation Letters*, vol. 5, pp. 269–273, 2006 (DOI: 10.1109/LAWP.2006.875888).

[7] H. Ma, B. Wang, Y. Chen, and K. J. Ray Liu, "Time-Reversal Tunneling Effects for Cloud Radio Access Network", *IEEE Transactions on Wireless Communications*, vol. 15, pp. 3030–3043, 2016 (DOI: 10.1109/TWC.2016.2515089).

[8] P. Liao, B. Hu, Z. Lin, Q. Wen, and L. Zheng, "Effect of Signal Characteristics on Focusing Property of Time Reversal Electromagnetic Wave", *2019 International Conference on Microwave and Millimeter Wave Technology (ICMMT)*, pp. 1–3, 2019 (DOI : 10.1109/ICMMT45702.2019.8992282).

[9] W. Lei and L. Yao, "Performance Analysis of Time Reversal Communication Systems", *IEEE Communications Letters*, vol. 23, pp. 680–683, 2019 (DOI: 10.1109/LCOMM.2019.2901484).

[10] P. Kosmas and C. M. Rappaport, "FDTD-based time reversal for microwave breast cancer Detection-localization in three dimensions", *IEEE Transactions on Microwave Theory and Techniques*, vol. 54, pp. 1921–1927, 2006 (DOI: 10.1109/TMTT.2006.871994).

[11] H. Terchoune, *et al.* "Investigation of space-time focusing of time reversal using FDTD", *2009 IEEE MTT-S International Microwave Symposium Digest*, pp. 273–276, 2009 (DOI: 10.1109/MWSYM.2009.5165686).

[12] X. Wei, W. Shao, S. Shi, Y. Cheng, and B. Wang, "An Optimized Higher Order PML in Domain Decomposition WLP-FDTD Method for Time Reversal Analysis", *IEEE Transactions on Antennas and Propagation*, vol. 64, pp. 4374–4383, 2016 (DOI: 10.1109/TAP.2016.2596899).

[13] W. Fan, Z. Chen and W. J. R. Hoefer, "Source Reconstruction From Wideband and Band-Limited Responses by FDTD Time Reversal and Regularized Least Squares", *IEEE Transactions on Microwave Theory and Techniques*, vol. 65, pp. 4785–4793, 2017 (DOI: 10.1109/TMTT.2017.2737991).

[14] J. G. Maloney and G. S. Smith, "The use of surface impedance concepts in the finite-difference time-domain method", *IEEE Transactions on Antennas and Propagation*, vol. 40, pp. 38–48, 1992 (DOI: 10.1109/8.123351).

[15] Y. Mao, A. Z. Elsherbeni, S. Li, and T. Jiang, "Surface impedance absorbing boundary for terminating FDTD simulations", *Applied Computational Electromagnetics Society Journal*, pp. 1035–1046, 2014 (https://journals.riverpublishers.com/index.php/ACES/article/view/10807/9029).

[16] Y. Mao, A. Z. Elsherbeni, T. Jiang, and S. Li, "Mixed surface impedance boundary condition for FDTD simulations", *IET Microwaves, Antennas and Propagation*, vol. 11, pp. 1197–1202, 2017 (DOI: 10.1049/iet-map.2016.0649).

[17] B. E. Anderson, M. Griffa, C. Larmat, T. J. Ulrich, and P. A. Johnson, "Time reversal", *Acoustics Today*, vol. 4, pp. 5–16, 2008 (https://acousticstoday.org/time-reversal-brian-e-anderson/).

[18] H. Vallon, "Focusing High-Power Electromagnetic Waves Using Time-Reversal", *PhD thesis*, University of Paris Saclay, 2016 (https://www.worldcat.org/title/focusing-high-power-electromagnetic-waves-using-time-reversal/oclc/948804731).

Zhigang Li received his B.Sc. in Information Engineering from the Nanjing University of Aeronautics and Astronautics, China, in 2015, and his M.Sc. in Electronic Systems for Embedded and Communicating Applications from École Nationale Supérieure d'Electrotechnique, d'Electronique, d'Informatique, d'Hydraulique et des Télécommunications (ENSEEIHT), France, in 2019. He is currently pursuing his Ph.D. at the University of Poitiers, France. His main research interests include electronics, electromagnetics, antennas, radar, and RF/mmW integrated circuit design.

E-mail: zhigang.li92@gmail.com

ESECA, Department of ENSEEIHT, National Polytechnic, Institute of Toulouse, Toulouse, France

Younes Aimer received his B.Sc. and M.Sc. in Electronics and Telecommunications from the University of Saida – Algeria in 2011 and 2013, respectively. He joined the University of Saida and Poitiers, where he received his co-supervision Ph.D. degree in Signal Processing and Telecommunications – Electronics, Microelectronics, Nanoelectronics, and Microwaves in 2019. He is presently a research engineer in Mines Saint-Etienne, Centre of Microelectronics in Provence at the Department of Flexible Electronics. His current research interests are digital communications, wireless and mobile communications, signal processing, electronic devices, IOT and wireless circuits.

E-mail: younes.aimer@emse.fr

Mines Saint-Etienne, Centre of Microelectronics in Provence, Department of Flexible Electronics, Gardanne, France

Tayeb H. C. Bouazza received his B.Sc. and M.Sc. in Electronics and Telecommunications from the University of Saida, Algeria in 2011 and 2013 respectively, and his Ph.D. in Electronics, Microelectronics, Nanoelectronics and Microwaves from XLIM Laboratory, University of Poitiers, France in 2021. His main research interests are in modelling nonlinear systems, signal processing and wireless communication.

E-mail: tayeb.habib.chawki.bouazza@univ-poitiers.fr

XLIM Laboratory UMR-CNRS 7252, Institute of Technology of Angouleme, University of Poitiers, Poitiers, France